Published in final edited form as:

Proc SPIE Int Soc Opt Eng. 2015 March ; 9417: . doi:10.1117/12.2082106.

Functional Connectivity Analysis in Resting State fMRI with Echo-State Networks and Non-Metric Clustering for Network Structure Recovery

Axel Wismüller[1,2,3,4,*], **Adora M. DSouza**[3,*,#], **Anas Z. Abidin**[1,2], **Xixi Wang**[1,2], **Susan K. Hobbs**[1], and **Mahesh B. Nagarajan**[1]

[1]Department of Imaging Sciences, University of Rochester Medical Center, NY, USA

[2]Department of Biomedical Engineering, University of Rochester, NY, USA

[3]Department of Electrical Engineering, University of Rochester, NY, USA

[4]Department of Clinical Radiology, Ludwig Maximilian University, Germany

Abstract

Echo state networks (ESN) are recurrent neural networks where the hidden layer is replaced with a fixed reservoir of neurons. Unlike feed-forward networks, neuron training in ESN is restricted to the output neurons alone thereby providing a computational advantage. We demonstrate the use of such ESNs in our mutual connectivity analysis (MCA) framework for recovering the primary motor cortex network associated with hand movement from resting state functional MRI (fMRI) data. Such a framework consists of two steps - (1) defining a pair-wise affinity matrix between different pixel time series within the brain to characterize network activity and (2) recovering network components from the affinity matrix with non-metric clustering. Here, ESNs are used to evaluate pair-wise cross-estimation performance between pixel time series to create the affinity matrix, which is subsequently subject to non-metric clustering with the Louvain method. For comparison, the ground truth of the motor cortex network structure is established with a task-based fMRI sequence. Overlap between the primary motor cortex network recovered with our model free MCA approach and the ground truth was measured with the Dice coefficient. Our results show that network recovery with our proposed MCA approach is in close agreement with the ground truth. Such network recovery is achieved without requiring low-pass filtering of the time series ensembles prior to analysis, an fMRI preprocessing step that has courted controversy in recent years. Thus, we conclude our MCA framework can allow recovery and visualization of the underlying functionally connected networks in the brain on resting state fMRI.

Keywords

resting-state functional MRI; functional connectivity; mutual connectivity analysis; echo state networks; non-metric clustering; Louvain method

[#] adora.dsouza@rochester.edu; phone 585-276-4775; University of Rochester, NY.
[*]Equal contributions.

1. INTRODUCTION

There has been significant growth in research aimed at exploring functional connectivity in the human brain at fine-grained spatial and temporal resolution scales, based on the acquisition capabilities provided by the most advanced contemporary in vivo neuro-imaging techniques, such as state-of-the-art fMRI [1]. Here, several analytic techniques such as seed-based functional connectivity analysis [2], principal component analysis (PCA) [3] independent component analysis (ICA) [4], Granger causality [5] etc. include assumptions of linearity or implicit time-series separability, which can obscure the characteristics of the complex system being investigated. Another drawback with such approaches is the transformation of the original high-dimensional imaging data into simpler lower-dimension representations, which further limits the interpretability of the results obtained from brain connectivity analysis.

We have previously proposed a computational framework involving non-linear mutual connectivity analysis [6] for recovering functionally connected networks in the brain from resting state fMRI data which circumvents the pitfalls of previously mentioned technique. Our approach involves network identification through large scale, model free, non-linear pair-wise cross-estimation [6] of fMRI time series followed by functional network identification through partitioning of the resulting affinity matrix with non-metric clustering. In this contribution, we explore the use of echo state networks (ESN) for constructing the pair-wise affinity matrix through evaluation of cross-estimation performance between pairs of pixel time series ensembles. Echo state networks (ESN) are recurrent neural networks where the hidden layer is replaced with a fixed reservoir of neurons [7]. Unlike feed-forward networks, neuron training in ESN is restricted to the output neurons alone thereby providing a computational advantage, which can be realized when applied to non-linear, dynamic systems such as functional networks in the human brain. The affinity matrix computed with these ESNs is then decomposed into the underlying network components through non-metric clustering with the Louvain method [8] for network recovery.

We demonstrate the applicability of our MCA framework to identifying and visualizing regions of the primary motor cortex network through analysis of resting-state fMRI data. It has been previously shown that frequency fluctuations (< 0.1 Hz) from regions of the motor cortex associated with hand movement are strongly correlated both within and across hemispheres [2]. We explore non-linear connectivity in time series ensembles from different regions of the primary motor cortex associated with hand movement, as discussed in the following sections. This work is embedded in our group’s endeavor to expedite ‘big data’ analysis in biomedical imaging by means of advanced pattern recognition and machine learning methods for computational radiology, e.g. [9–39].

2. DATA

Functional MRI data was acquired using a 1.5T GE SIGNA™ whole-body MRI scanner (GE, Milwaukee, WI, USA) from a cohort of four healthy subjects aged between 25 to 28 years (3 males and 1 female). Two fMRI sequences were performed on all subjects, one under resting-state conditions and the other involving a finger-tapping task that stimulated

the primary motor cortex. The purpose of the task sequence was to enable localization of the left motor cortex (LMC), right motor cortex (RMC) and the supplementary motor area (SMA) regions of the primary motor cortex network, which served as ground truth. All fMRI (EPI-BOLD) sequences were acquired using TE = 40ms, TR = 500ms, and FA = 90°. 512 fMRI scans were acquired from two slice locations that corresponded to the motor cortex; each image had a slice thickness of 10 mm and an in-plane pixel resolution of 3.75 mm x 3.75 mm. The first 24 time points of fMRI data were discarded to avoid any impact on the data analysis by initial saturation effects.

3. METHODS

3.1 Preprocessing fMRI data

Registration of the fMRI time series was performed to compensate for motion artifacts. Subsequent linear de-trending eliminated signal drifts caused during acquisition. We specifically note that our pre-processing of resting state fMRI data does not include low-pass filtering at a cut-off frequency of 0.08 Hz, a step that has attracted controversy in recent years [40]. Finally, the time-courses were further normalized to zero mean and unit standard deviation to focus on signal dynamics rather than amplitude [41]

3.2 Pair-wise affinity matrix computation with ESN

Our first step is to build a pair-wise affinity/similarity matrix $\mathbf{A}$ for all time series from the brain on a single fMRI slice. The similarity measure used in this study is based on cross-estimation performance. Given N pixels, the pair-wise affinity between two pixel time series $\boldsymbol{x}$ and $\boldsymbol{y}$ (where $\boldsymbol{x} = (x(1),\ldots,x(t))$, and $\boldsymbol{y} = (y(1),\ldots,y(t))$) describes the degree of their dynamic coupling as a measure of how well one can estimate $\boldsymbol{y}$ given $\boldsymbol{x}$. For this purpose, we use ESNs as previously described in [7]. Briefly, ESNs are recurrent neural networks that have a reservoir of M sparsely connected neurons whose weights are randomly assigned, fixed and do not require any training and a set of output neurons that are trained such that the error between response of the network and desired value is minimum [7]. During the training phase of the ESN, this reservoir of neurons is driven by the training subset of $\boldsymbol{x}$, i.e. $\boldsymbol{x_{TR}}$, the state of the neurons in the reservoir is given by $\boldsymbol{U}$, and the training subset of the desired target $\boldsymbol{y_{TR}}$ and reservoir output is linearly combined with a set of output neurons to produce the final ESN output. The output weights are selected such that the ESN output best replicates $\boldsymbol{y_{TR}}$. During the test phase, the test subset of $\boldsymbol{x}$, i.e. $\boldsymbol{x_T}$, now drives the ESN and produces an estimate of $\boldsymbol{y_T}$, i.e. $\hat{\boldsymbol{y}}_{\boldsymbol{T}}$. Now, the entry $\mathbf{A}_{\boldsymbol{X,Y}}$ of the affinity matrix is chosen as the Pearson correlation coefficient computed between $\hat{\boldsymbol{y}}_{\boldsymbol{T}}$ and $\boldsymbol{y_T}$.

The number of output neurons is N, and the number of input neurons is set to 2, namely one for the time series $\boldsymbol{x}$ and the other for the bias term [42]. We design the ESN network to predict N of the time series $\mathbf{Y} = \{\boldsymbol{y}_1,\ldots,\boldsymbol{y}_N\}$ where, $\boldsymbol{y}_n = (y_n(1),\ldots,y_n(t))$ independently of each other, where $n = 1,\ldots,N$. Using one time series, ESNs can be applied with the underlying assumption that the output can in fact be estimated from the given input. For the given fMRI data, a small reservoir is used to prevent over-fitting. In this study, we use a reservoir of 35 neurons, with output feedback. Smaller reservoirs could not be used owing to their inability to keep up with the abrupt, high frequency changes in the time series. We used

60 percent of the time series for training and the remaining 40 percent for testing. We used non-spiking, leaky integrator neurons and output feedback with a scaling factor of 0.2. Leaky integrator neurons [43] are used when the network should have memory in order to model continuously changing dynamics. Here, the amount by which the previous state influences the current state is given by the leakage parameter *a*, see equation (2) below.

The state update equations are as follows –

$$\overrightarrow{\boldsymbol{u}}\ (t)=\boldsymbol{f}(\mathbf{W}_{\text{in}}\,[x(t):b(t)])+\mathbf{W}\boldsymbol{u}(t-1)+\mathbf{W}_{\text{back}}\boldsymbol{y}(t)), \quad (1)$$

$$\boldsymbol{u}(t)=(1-a)\,\boldsymbol{u}(t-1)+a\ \overrightarrow{\boldsymbol{u}}\ (t), \quad (2)$$

where $\mathbf{W}_{\text{in}}$ is the input weight matrix with dimension M x 2, $\mathbf{W}$ is an M x M reservoir weight matrix and $\mathbf{W}_{\text{back}}$ is an M x N output weight matrix, $\boldsymbol{y}(t) = (y_1(t),\ldots y_N(t))$ and $\boldsymbol{u}(t) = (u_1(t),\ldots\ u_M(t))$. The notation [:] represents the concatenation of the input and the bias. The function $\boldsymbol{f} = (f_1,\ldots,f_N)$ is the activation function of the reservoir neurons, $\boldsymbol{u}(t)$ is the current state of the reservoir neurons, $b(t)$ is the bias term, and a the leakage rate; when $a = 1$, $\boldsymbol{u}(t) = \grave{\boldsymbol{u}}(t)$, and the system has no memory. When $a = 0$, $\boldsymbol{u}(t) = \boldsymbol{u}(t\text{-}1)$, which means that the state of the system does not change. The parameter a can be varied between 0 and 1, and finally,

$$\boldsymbol{y}(t)=\boldsymbol{f}_{\text{out}}\,(\mathbf{W}_{\text{out}}\,[x(t):b(t):\boldsymbol{u}(t)]), \quad (3)$$

where $\mathbf{W}_{\text{out}}$ is the output matrix, which is of dimension N x ($M + 2$). The function $\boldsymbol{f}_{\text{out}}$ is the activation function of the output neurons. The notation [: :] represents the concatenation of the input, bias, and reservoir states. As such, the output can be computed from the input and the reservoir states.

3.3 Louvain method for non-metric clustering

From the affinity matrix **A** we find the network structure using non-metric clustering such as Louvain method [8]. The Louvain method aims to find high modularity clusters in networks, where modularity is the measure of the quality of a partition of the network into different clusters. Thus, a complex network is decomposed into clusters with strong intra-community links and weak inter-community links. Modularity is given by:

$$Q=\tfrac{1}{2m}\textstyle\sum_{i,j}\left[A_{ij}-\tfrac{k_i k_j}{2m}\right]\,\delta\,(C_i,C_j) \quad (4)$$

where A_{ij} is the weight that represents the similarity between nodes i and j,

$$k_i = \sum_j A_{ij} \quad (5)$$

is the sum of weights in A_{ij} that are attached to vertex i, i is in community C_i, $\delta(u,v) = 1$ when $u = v$, and 0 otherwise, and

$$m = \frac{1}{2} \sum_{ij} A_{ij} \quad (6)$$

Thus, a complex network, such as the brain, is decomposed into clusters, which are functionally connected networks in the brain, with strong intra-community links and weak inter-community links. The maximum modularity is obtained by an iterative process during which different nodes of the network are merged into larger communities if the modularity is improved as a consequence. The process is stopped when no further improvement in modularity can be achieved. Further details to the Louvain method can be found in [8].

Applying Louvain clustering on the affinity matrix A results in large and improper clusters. This could be due to the fact that even 'noise' is considered as weak connections when clustering. In order to avoid this, we use an approach frequently applied in spectral clustering [44] to make the affinity matrix sparser. Specifically, we only consider the k most similar nodes for any given node i. In this study we have also investigated the effect of using different percentages of the nearest neighbors. The clustering results obtained by our methods are evaluated against the ground truth using the Dice coefficient [45].

All procedures were implemented using MATLAB 8.1 (MathWorks Inc., Natick, MA, 2013). The Louvain method implementation was taken from [46] and echo state network from [47].

4. RESULTS

The behavior of the ESN during the training and testing phase is demonstrated for an example pair of time series in Figure 1. During the training phase, the output weights of the ESN are optimized for maximum resemblance between the desired and actual output. As expected, when the training portion of the time series is used as input for the trained ESN, the produced output is quite similar to the desired output (here, the training portion of the second time series), as seen in Figure 1 (left pane). However, during the test phase, greater differences between the desired and actual output of the trained ESN are noted, as expected.

Figure 2 shows the results of the primary motor cortex network recovery with the Louvain method along with the ground truth. The Dice coefficient between the ground truth and the results achieved with our MCA approach was 0.59. The results show clear visualization of the LMC, RMC and SMA regions.

Table 1 enumerates the results obtained for the different subjects using our analysis. The highest dice coefficient obtained is 0.55.

5. NEW AND BREAKTHROUGH WORK

We present a computational framework for analysis of functional connectivity in the brain from resting state fMRI data for purposes of recovering the underlying network structure while avoiding information loss-inducing assumptions such as linearity, implicit time series separability etc. To this end, we propose to use non-linear mutual connectivity analysis (MCA) to evaluate the pair-wise cross-estimation/prediction quality between resting state fMRI time series acquired from the brain. Our results, as demonstrated with the primary motor cortex network in Figure 2, suggest that such a computational framework can also reveal valuable information concerning the underlying network structure. In this contribution, we specifically focus on the use of ESNs [7] for evaluating cross-estimation capabilities between fMRI pixel time series while constructing the pair-wise affinity matrix. In addition, using ESN, where training is restricted to the output neurons, provides a huge computational advantage as compared to using feed-forward networks. Our results suggest that such ESNs are more robust to the high frequency components in such resting state fMRI data and allow for network recovery without requiring prior low-pass filtering of the data, which has been a source of controversy in the literature [40].

6. CONCLUSION

We present an MCA framework for analysis of functional connectivity in the brain from resting state fMRI data, using ESNs to establish network connectivity through pair-wise cross-estimation performance of time series, and non-metric clustering with the Louvain method to recover network structure. The results observed in our study demonstrates that our methodology constitutes a model-free approach to recovering the network structure of the primary motor cortex, where its robustness to high frequency components in fMRI data suggests that prior low-pass filtering is not required for this task.

This work is not being and has not been submitted for publication or presentation elsewhere.

Acknowledgments

This research was funded by the National Institutes of Health (NIH) Award R01-DA-034977. The content is solely the responsibility of the authors and does not necessarily represent the official views of the National Institute of Health. This work was conducted as a Practice Quality Improvement (PQI) project related to American Board of Radiology (ABR) Maintenance of Certificate (MOC) for Prof. Dr. Axel Wismüller. The authors would like to thank Prof. Dr. Dorothee Auer at the Institute of Neuroscience, University of Nottingham, UK, for her assistance with the fMRI data acquisition process. The authors would also like to thank Dr. Lutz Leistritz and Prof. Dr. Herbert Witte of Bernstein Group for Computational Neuroscience Jena, Institute of Medical Statistics, Computer Sciences, and Documentation, Jena University Hospital, Friedrich Schiller University Jena, Germany, Dr. Oliver Lange and Prof. Dr. Maximilian F. Reiser of the Institute of Clinical Radiology, Ludwig Maximilian University, Munich, Germany for their support.

References

1. Margulies DS, Böttger J, Long X, Lv Y, Kelly C, Schäfer A, Goldhahn D, Abbushi A, Milham MP, Lohmann G, Villringer A. Resting developments: a review of fMRI post-processing methodologies for spontaneous brain activity. Magnetic Resonance Materials in Physics, Biology and Medicine. 2010; 23(5–6):289–307.

2. Biswal B, Yetkin FZ, Haughton VM, Hyde JS. Functional connectivity in the motor cortex of resting human brain using echo-planar MRI. Magnetic Resonance in Medicine. 1995; 34:537–541. [PubMed: 8524021]
3. Zhong Y, Wang H, Lu G, Zhang Z, Jiao Q, Liu Y. Detecting functional connectivity in fMRI using PCA and regression analysis. Brain Topography. 2009; 22(2):134–44. [PubMed: 19408112]
4. Beckmann CF, DeLuca M, Devlin JT, Smith SM. Investigations into resting-state connectivity using independent component analysis. Philosophical Translations of the Royal Society B: Biological Sciences. 2005; 360:1001–1013.
5. Friston K, Moran R, Seth AK. Analysing connectivity with Granger causality and dynamic causal modelling. Current Opinion in Neurobiology. 2013; 23(2):172–8. [PubMed: 23265964]
6. Wismüller A, Lange O, Auer DP, Leinsinger G. Model-free functional MRI analysis for detecting low-frequency functional connectivity in the human brain. Proceedings of SPIE Medical Imaging. 2010; 7624:1M1–8.
7. Jaeger H, Haas H. Harnessing nonlinearity: Predicting chaotic systems and saving energy in wireless communication. Science. 2004; 304:78–80. [PubMed: 15064413]
8. Blondel VD, Guillame J-L, Lambiotte R, Lefebvre E. Fast unfolding of communities in large networks. Journal of Statistical Mechanics: Theory and Experiment. 2008:P10008.
9. Bunte K, Hammer B, Wismüller A, Biehl M. Adaptive local dissimilarity measures for discriminative dimension reduction of labeled data. Neurocomputing. 2010; 73(7):1074–1092.
10. Wismüller A, Vietze F, Dersch DR. Segmentation with neural networks. Handbook of Medical Imaging. 2000:107–126.
11. Leinsinger, G., Schlossbauer, T., Scherr, M., Lange, O., Reiser, M., Wismüller, A. Eur Radiol. Vol. 16. Springer-Verlag; 2006. Cluster analysis of signal-intensity time course in dynamic breast MRI: does unsupervised vector quantization help to evaluate small mammographic lesions?; p. 1138-1146.
12. Wismüller A, Vietze F, Behrends J, Meyer-Baese A, Reiser M, Ritter H. Fully automated biomedical image segmentation by self-organized model adaptation. Neural Networks. 2004; 17(8):1327–1344. [PubMed: 15555869]
13. Hoole P, Wismüller A, Leinsinger G, Kroos C, Geumann A, Inoue M. Analysis of tongue configuration in multi-speaker, multi-volume MRI data. Proc 5th Semin Speech Prod Model Data CREST Work Model Speech Prod Mot Plan Articul Model. 2000:157–160.
14. Wismüller, A. Ph D thesis. Technical University of Munich, Department of Electrical and Computer Engineering; 2006. Exploratory Morphogenesis (XOM): a novel computational framework for self-organization.
15. Wismüller, A., Dersch, DR., Lipinski, B., Hahn, K., Auer, D. “A neural network approach to functional MRI pattern analysis—clustering of time-series by hierarchical vector quantization,” [ICANN 98]. Springer; London: 1998. p. 857-862.
16. Wismüller A, Vietze F, Dersch DR, Behrends J, Hahn K, Ritter H. The deformable feature map-a novel neurocomputing algorithm for adaptive plasticity in pattern analysis. Neurocomputing. 2002; 48(1):107–139.
17. Behrends, J., Hoole, P., Leinsinger, GL., Tillmann, HG., Hahn, K., Reiser, M., Wismüller, A. “A segmentation and analysis method for MRI data of the human vocal tract,” [Bildverarbeitung für die Medizin 2003]. Springer; Berlin Heidelberg: 2003. p. 186-190.
18. Wismüller A, Dersch DR. Neural network computation in biomedical research: chances for conceptual cross-fertilization. Theory Biosci. 1997; 116(3):229–240.
19. Bunte K, Hammer B, Villmann T, Biehl M, Wismüller A. Exploratory Observation Machine (XOM) with Kullback-Leibler Divergence for Dimensionality Reduction and Visualization. ESANN. 2010; 10:87–92.
20. Wismüller, A., Vietze, F., Dersch, DR., Hahn, K., Ritter, H. “The deformable feature map—adaptive plasticity for function approximation,” [ICANN 98]. Springer; London: 1998. p. 123-128.
21. Wismüller, A. Advances in Self-Organizing Maps. Springer; Berlin Heidelberg: 2009. The exploration machine--a novel method for data visualization; p. 344-352.

22. Meyer-Bäse, A., Jancke, K., Wismüller, A., Foo, S., Martinetz, T. Eng Appl Artif Intell. Vol. 18. Elsevier; 2005. Medical image compression using topology-preserving neural networks; p. 383-392.
23. Huber, MB., Nagarajan, M., Leinsinger, G., Ray, LA., Wismüller, A. SPIE Med Imaging 7624, 762410. International Society for Optics and Photonics; 2010. Classification of interstitial lung disease patterns with topological texture features.
24. Wismüller A. The exploration machine: a novel method for analyzing high-dimensional data in computer-aided diagnosis. SPIE Med Imaging. 2009:72600G–72600G.
25. Bunte, K., Hammer, B., Villmann, T., Biehl, M., Wismüller, A. Neurocomputing. Vol. 74. Elsevier; 2011. Neighbor embedding XOM for dimension reduction and visualization; p. 1340-1350.
26. Wismüller, A. Advances in Self-Organizing Maps. Springer; Berlin Heidelberg: 2009. A computational framework for nonlinear dimensionality reduction and clustering; p. 334-343.
27. Huber, MB., Nagarajan, MB., Leinsinger, G., Eibel, R., Ray, LA., Wismüller, A. Med Phys. Vol. 38. American Association of Physicists in Medicine; 2011. Performance of topological texture features to classify fibrotic interstitial lung disease patterns; p. 2035-2044.
28. Wismüller, A., Verleysen, M., Aupetit, M., Lee, JA. ESANN. 2010. Recent Advances in Nonlinear Dimensionality Reduction, Manifold and Topological Learning.
29. Wismüller, A., Meyer-Baese, A., Lange, O., Reiser, MF., Leinsinger, G. Med Imaging, IEEE Trans. Vol. 25. IEEE; 2006. Cluster analysis of dynamic cerebral contrast-enhanced perfusion MRI time-series; p. 62-73.
30. Twellmann T, Saalbach A, Müller C, Nattkemper TW, Wismüller A. Detection of suspicious lesions in dynamic contrast enhanced MRI data. Eng Med Biol Soc 2004 IEMBS'04 26th Annu Int Conf IEEE. 2004; 1:454–457.
31. Schlossbauer, T., Leinsinger, G., Wismüller, A., Lange, O., Scherr, M., Meyer-Baese, A., Reiser, M. Invest Radiol. Vol. 43. NIH Public Access; 2008. Classification of small contrast enhancing breast lesions in dynamic magnetic resonance imaging using a combination of morphological criteria and dynamic analysis based on unsupervised vector-quantization; p. 56
32. Otto TD, Meyer-Baese A, Hurdal M, Sumners D, Auer D, Wismüller A. Model-free functional MRI analysis using cluster-based methods. AeroSense. 2003; 2003:17–24.
33. Varini C, Nattkemper TW, Degenhard A, Wismüller A. Breast MRI data analysis by LLE. Neural Networks, 2004 Proceedings 2004 IEEE Int Jt Conf. 2004; 3:2449–2454.
34. Huber, MB., Lancianese, SL., Nagarajan, MB., Ikpot, IZ., Lerner, AL., Wismüller, A. Biomed Eng IEEE Trans. Vol. 58. IEEE; 2011. Prediction of biomechanical properties of trabecular bone in MR images with geometric features and support vector regression; p. 1820-1826.
35. Meyer-Base A, Pilyugin SS, Wismüller A. Stability analysis of a self-organizing neural network with feedforward and feedback dynamics. Neural Networks, 2004 Proceedings 2004 IEEE Int Jt Conf. 2004; 2:1505–1509.
36. Schlossbauer, T., Kallergi, M., Reiser, MF., Wismüller, A., Meyer-Baese, A., Lange, O., Leinsinger, G. J Electron Imaging. Vol. 15. International Society for Optics and Photonics; 2006. Segmentation and classification of dynamic breast magnetic resonance image data; p. 13020
37. Nagarajan, MB., Huber, MB., Schlossbauer, T., Leinsinger, G., Krol, A., Wismüller, A. Mach Vis Appl. Vol. 24. Springer; Berlin Heidelberg: 2013. Classification of small lesions in dynamic breast MRI: eliminating the need for precise lesion segmentation through spatio-temporal analysis of contrast enhancement; p. 1371-1381.
38. Nagarajan, MB., Huber, MB., Schlossbauer, T., Leinsinger, G., Krol, A., Wismüller, A. J Med Biol Eng. Vol. 33. NIH Public Access; 2013. Classification of Small Lesions in Breast MRI: Evaluating The Role of Dynamically Extracted Texture Features Through Feature Selection.
39. Wismüller, A., Meyer-Bäse, A., Lange, O., Auer, D., Reiser, MF., Sumners, D. J Biomed Inform. Vol. 37. Academic Press; 2004. Model-free functional MRI analysis based on unsupervised clustering; p. 10-18.
40. Davey CE, Grayden DB, Egan GF, Johnston LA. Filtering induces correlation in fMRI resting state data. NeuroImage. 2013; 64:728–740. [PubMed: 22939874]
41. Wismüller A, Lange O, Dersch DR, Leinsinger GL, Hahn K, Pütz B, Auer D. Cluster analysis of biomedical image time-series. International Journal of Computer Vision. 2002; 46:103–128.

42. Lukoševičius, M. Neural Networks: Tricks of the Trade. Springer; Berlin Heidelberg: 2012. A practical guide to applying echo state networks; p. 659-686.

43. Jaeger, H. The “echo state” approach to analysing and training recurrent neural networks-with an erratum note,”. Vol. 148. Bonn, Germany: German National Research Center for Information Technology GMD Technical Report; 2001. p. 34

44. von Luxburg, U. Technical Report TR-149. Max Planck Institute for Biological Cybernetics; 2006. A tutorial on spectral clustering.

45. Dice LR. Measures of the Amount of Ecologic Association Between Species. Ecology. 1945; 26(3):297–302.

46. Scherrer, A. Community Detection algorithm based on Louvain method (Version 1.0) [software]. Available from http://perso.uclouvain.be/vincent.blondel/research/Community_BGLL_Matlab.zip

47. Fraunhofer, IAIS. Quintessential documentation of the ESN learning toolbox Version 1.0, 2007.

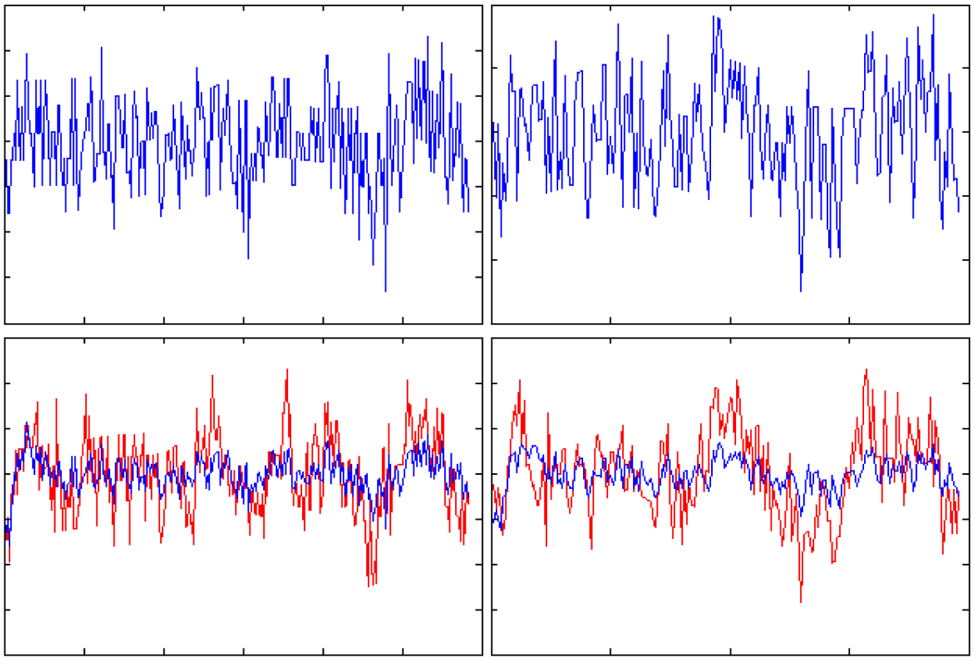

Figure 1.

Top Left: Portion of a sample time series used for training the ESN; Bottom Left: Output of trained ESN for the input shown in top left pane; the actual output is shown in blue while the expected output is shown in red; Top Right: Remainder of the same sample time series used for testing the ESN; Bottom Right: Output of trained ESN for the input shown in the top right pane; the actual output is shown in blue while the expected output is shown in red.

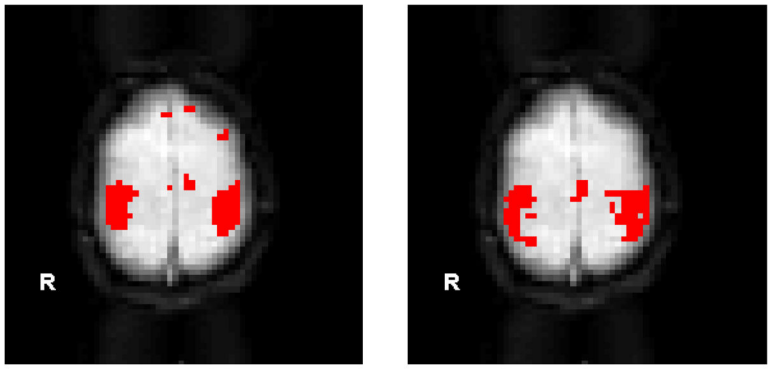

Figure 2.

Comparison of ground truth (left) and results of our model free MCA approach (right), in recovering and visualizing regions of the primary motor cortex (highlighted in red). As seen here, our MCA approach is able to recover the primary motor cortex network with close similarity to the ground truth.

Table 1

Dice coefficients (Mean ± Standard deviation) achieved for the different patients over 10 iterations of the algorithm. The best result overall is highlighted in bold. Here the number k of most similar nodes to a given node is chosen as 2%.

Subject Number	Slice Number	Dice Coefficient
1	1	0.44 ± 0.083
	2	**0.55 ± 0.067**
2	1	0.44 ± 0.04
	2	0.32 ± 0.089
3	1	0.51 ± 0.028
	2	0.31 ± 0.045
4	1	0.28 ± 0.029
	2	0.25 ± 0.062